Ultrafast Optical Parametric Pumping of Magnetization Reorientation and Precessional Dynamics in $DyFe_2/YFe_2$ Exchange Springs

L. R. Shelford,[1,*] Y. Liu,[1] U. Al-Jarah,[1] P. A. J. de Groot,[2] G. J. Bowden,[2] R. C. C. Ward,[3] and R. J. Hicken[1]
[1]School of Physics, University of Exeter, Stocker Road, Exeter, Devon EX4 4QL, United Kingdom
[2]School of Physics and Astronomy, University of Southampton, Southampton SO17 1BJ, United Kingdom
[3]Clarendon Laboratory, University of Oxford, Parks Road, Oxford OX1 3PU, United Kingdom
(Received 1 June 2013; revised manuscript received 2 December 2013; published 7 August 2014)

The magnetization dynamics of a wound $[DyFe_2(20\ \text{Å})/YFe_2(80\ \text{Å})]_{\times 40}$ exchange spring multilayer have been explored in optical pump probe experiments. Ultrafast optical heating was used to modify the magnetic parameters of the multilayer, while the time resolved magneto-optical Kerr effect was used to probe its response. Although the probe signal is dominated by precession and winding of the exchange spring within the soft YFe_2 layer, reorientation of the $DyFe_2$ hard-layer magnetization is detected on time scales less than 100 ps. Micromagnetic simulations reproduce the main features of the experimental data and indicate a dramatic optically induced reduction of the hard-layer anisotropy. The results establish the feasibility of switching a spring system by means of parametric excitation.

DOI: 10.1103/PhysRevLett.113.067601 PACS numbers: 76.50.+g, 75.30.Et, 75.40.Gb, 76.70.Hb

A variety of physical systems display instability and sudden deformation when subject to a critical load or field. Familiar examples are the Euler strut and the Fréedericksz transition in liquid crystals. The critical load or field depends upon the material parameters of the system, such as the Young's modulus of the strut or the elastic constant of the liquid crystal, and the pinning parameters at the boundaries. Parametric excitation may therefore be used to drive the deformation of the system, leading to new functionality in electromechanical and electro-optical device applications.

Exchange-coupled superlattices containing alternating hard and soft magnetic layers exhibit analogous behavior. The large magnetic anisotropy of the hard layers and interfacial exchange coupling pin the magnetization of the soft layers to the hard-layer easy axis. When a magnetic field H is applied antiparallel to the soft-layer magnetization, the magnetic state is unchanged until H exceeds a critical value H_{bend}. If the hard-layer magnetization remains rigid and fixed, H_{bend} takes the form [1]

$$H_{\text{bend}} = \frac{2K}{M} + \frac{\pi^2}{N^2}\frac{aA}{2M}, \tag{1}$$

where K and M are the uniaxial anisotropy constant and magnetization, A is the exchange constant, a is the lattice constant, and N is the number of unit cells within the soft layer. When H exceeds H_{bend} but is less than the switching field of the hard layer, a wound exchange spring is formed in each soft layer. The magnetization remains pinned at the interface with the hard layer and exhibits maximum rotation at the center of the soft layer. For a hard layer of finite anisotropy and exchange stiffness the spring may also extend into the hard layer. The system can be driven from equilibrium by modification of the K, M, and A values of either the hard or soft layer.

Exchange spring multilayers are of great interest for high density [2,3] and heat assisted magnetic recording [4], while antiferromagnetically coupled RFe_2 (R denotes rare-earth metal) multilayers exhibit tunable coercivity [5,6] and giant magnetoresistance [7]. Ferromagnetic resonance has been measured and simulated in ferromagnetically coupled [8,9] and antiferromagnetically coupled [10] exchange springs, while microwave assisted switching has been simulated [11,12]. However, the parametric excitation of exchange springs by ultrafast optical pulses has not been explored.

In this Letter we explore the optically induced magnetization dynamics of a $[DyFe_2/YFe_2]_{\times 40}$ multilayer prepared in a wound spring state. The data are compared with micromagnetic simulations that allow the role of different magnetic parameters to be explored. Precession and winding of the exchange spring within the soft YFe_2 layer are shown to dominate the observed response. However, reorientation of the $DyFe_2$ hard-layer magnetization is also detected on time scales less than 100 ps, confirming that the hard-layer anisotropy is dramatically reduced. The results establish the feasibility of switching exchange springs by optical parametric excitation.

A $C15$ Laves phase $[DyFe_2(20\ \text{Å})/YFe_2(80\ \text{Å})]_{\times 40}$ superlattice of (110) orientation was grown on a $(11\bar{2}0)$ sapphire substrate with 75 Å Nb buffer and 20 Å Fe seed layers by molecular beam epitaxy [13]. The $DyFe_2$ is ferrimagnetic with net magnetization parallel to the Dy moment. The large spin-orbit coupling associated with the Dy $4f$ moments leads to a fourfold magnetocrystalline anisotropy and also a large strain-induced uniaxial anisotropy that dominates the anisotropy of the superlattice

within the plane [14,15]. The anisotropy of the $DyFe_2$ layers is strongly temperature dependent, so that the coercivity of the superlattice varies from 10 T to 1 T in the range 10–300 K [14,16,17]. The YFe_2 is magnetically soft and largely ferromagnetic with only a small moment on the Y sites. Interlayer coupling between the $DyFe_2$ and YFe_2 is dominated by Fe-Fe ferromagnetic exchange so that the superlattice forms a giant ferrimagnet [Fig. 1(b)] in zero external field. For the 4:1 YFe_2:$DyFe_2$ thickness ratio, the net magnetization lies parallel to that of the YFe_2.

Magnetization dynamics were studied by time-resolved magneto-optical Kerr effect (TRMOKE) measurements, using an amplified Ti:sapphire pulsed laser source with 50 fs pulsewidth and 100 kHz repetition rate. The linearly polarized 400 nm wavelength pump and 800 nm wavelength probe beams were incident normal and at 45° to the sample surface, respectively, and focused to 80 μm and 25 μm full width at half maximum spot diameters. An external field was applied in the plane of incidence and parallel to the $[1\bar{1}0]$ easy axis.

Figure 1(a) shows a minor MOKE hysteresis loop recorded at 633 nm wavelength with the applied field parallel to the $[1\bar{1}0]$ easy axis. The persistence of the high field MOKE signal as the field is reduced to zero indicates that the state at the −4 kOe maximum field is the giant

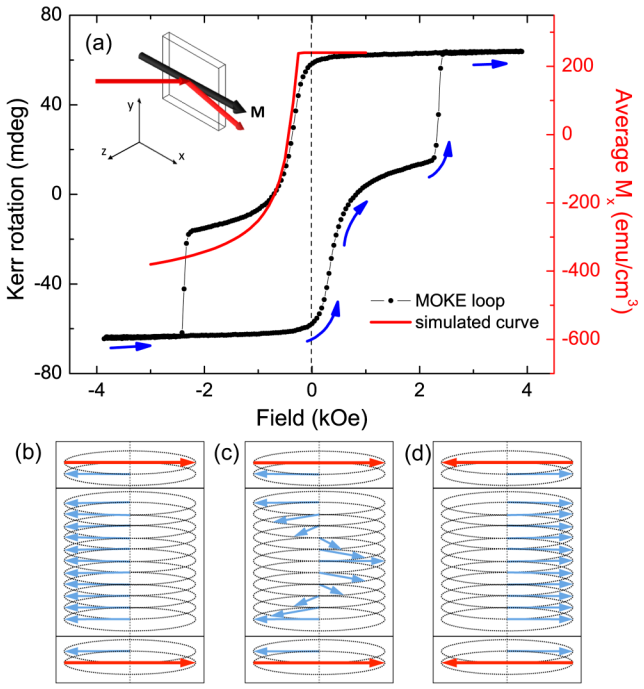

FIG. 1 (color online). (a) MOKE hysteresis loop recorded at 633 nm wavelength (black) and simulated magnetization curve (red) of the $DyFe_2/YFe_2$ multilayer $[1\bar{1}0]$ easy axis, with measurement geometry inset. Blue arrows show the direction of field sweep. (b)–(d) Reversal process, where blue and red arrows represent Fe and Dy moments respectively (the weak Y moments are omitted for clarity).

ferrimagnetic state [Fig. 1(b)]. As the field is increased from −4 to +2.5 kOe, a reversible curve characteristic of the formation of an exchange spring is obtained [see Fig. 1(c)]. At ~2.5 kOe the $DyFe_2$ magnetization switches while the exchange spring within the YFe_2 unwinds, reducing the net magnetization of the superlattice. However, the MOKE signal is observed to increase because the magneto-optical constants of YFe_2 and $DyFe_2$ have opposite sign, at both 633 nm and 800 nm wavelength. The harder $DyFe_2$ moments would switch again if a higher field was applied, forming a high field exchange spring state [18].

Magnetization dynamics are excited by a sudden reorientation of the effective field following laser absorption and modification of the magnetic parameters [19,20]. Here the external field was applied along the $[1\bar{1}0]$ easy axis to avoid perturbing the remanent giant ferrimagnetic state by reduction of the magnetization and anisotropy. Consequently, no oscillatory precessional dynamics were observed in the giant ferrimagnetic state. The response was also observed to be insensitive to the polarization of the pump beam after about the first 100 fs.

Figure 2(a) shows TRMOKE data acquired with varied bias field strength with the pump laser fluence fixed at 2.0 mJ/cm^2. In (b) the same data is presented on a shorter time scale where a slowly varying background on which the oscillations are superposed has been fitted and subtracted. The signal measured at negative time delays of up to 4 ps before the arrival of the pump pulse had zero value, confirming that the system returns to the equilibrium state after each subsequent pump pulse. No oscillatory signal is observed for the giant ferrimagnetic state at −3.1 kOe. After a sharp rise on a time scale of about 0.5 ps, the signal typically increases by a further 20% until reaching a maximum at a time delay of about 70 ps, before recovering more slowly. The maximum at longer time delay may be due to a slight reorientation of the hard-layer magnetization if the applied field is slightly misaligned from the easy axis, or a result of the different relaxation times of the magnetization in the constituent layers. Hysteresis loops recorded in the presence of the pump beam at a time delay of 70 ps showed that the change in Kerr rotation corresponds to about 20% of the loop height in the absence of the pump (see Supplemental Material [21] for details). All measurements performed in the wound spring state, 0.65–1.5 kOe, show three significant features. First, there is a large amplitude, heavily damped oscillatory response. The maximum peak-to-peak oscillation amplitude of ~5 mdeg corresponds to about 11% of the maximum MOKE signal (45 mdeg). Fourier power spectra of the time domain data with slowly varying background subtracted [Fig. 2(c)] show that the oscillation frequency increases from ~4 to 8 GHz with increasing field. Second, the sign of the background signal (slow variation on 100's ps time scale) changes with increasing field. Third, there is a small

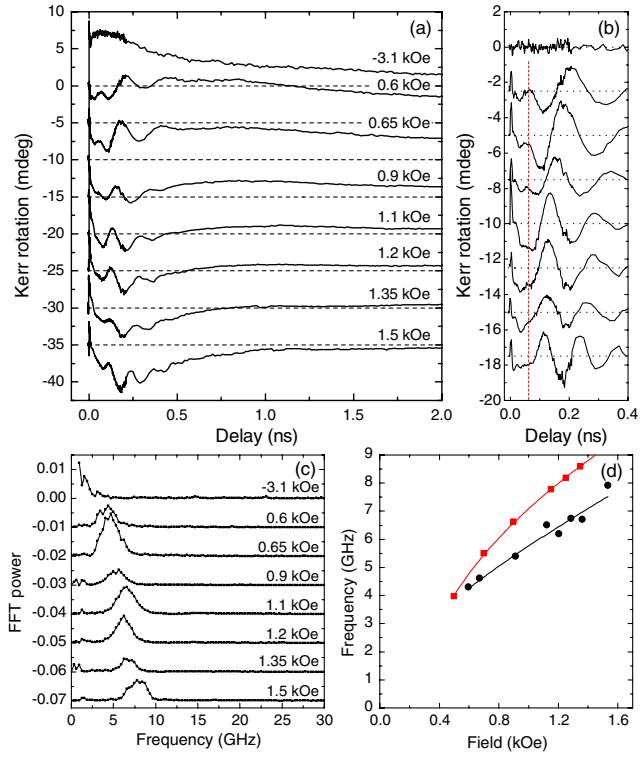

FIG. 2 (color online). (a) and (b) TRMOKE data as a function of applied field strength for pump fluence of 2.0 mJ/cm^2. In (b) the data is presented with the subtraction of the slowly varying background and on a shorter time delay to highlight an inflection at ~60 ps delay, indicated by a vertical dashed line. (c) Power spectra of the time domain data, and (d) frequency of largest amplitude mode as a function of bias field from experiment (black circles) and simulation (red squares).

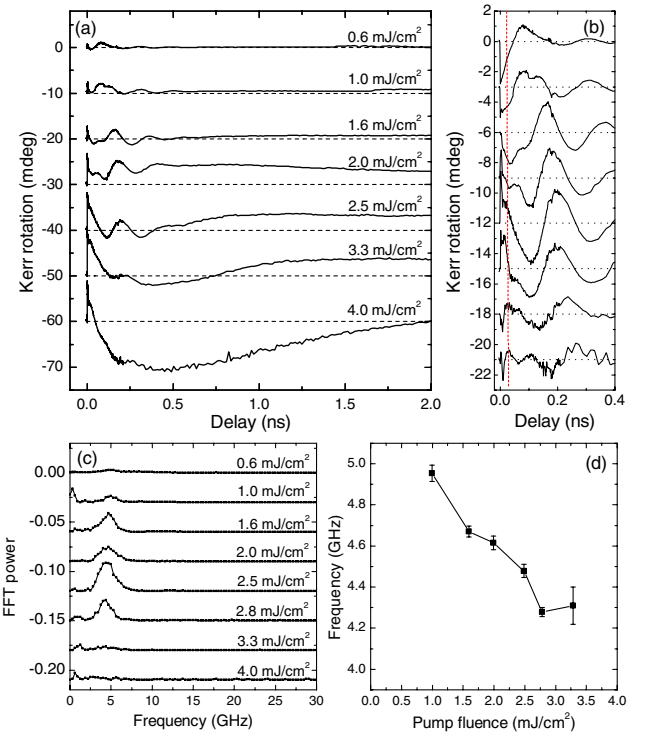

FIG. 3 (color online). (a) and (b) TRMOKE data for different pump fluences after the bias field applied along the $[1\bar{1}0]$ axis was reduced from −4 to +0.65 kOe. (c) Power spectra and (d) frequency for different pump fluences.

inflection at ~60 ps delay, highlighted by a vertical dashed line in Fig. 2(b). The feature is most clear at 0.65 kOe, but is visible in all TRMOKE data at the same time delay.

TRMOKE data recorded at +0.65 kOe with varied pump fluence are presented in the same format in Fig. 3. The oscillation amplitude increases with fluence up to a maximum at 2.5 mJ/cm^2, before decreasing rapidly, due to an increase in damping associated with higher optically induced temperatures and/or nonlinear magnetization dynamics. Power spectra reveal that the frequency falls by about 15% as the pump fluence is increased across the measured range. The slowly varying background signal is also strongly fluence dependent. For the highest fluence the minimum at ~0.5 ns has an amplitude equivalent to ~40% of the MOKE loop height. The measured noise also increases significantly for the highest fluence, suggesting the possible onset of stochastic character. However, the peak feature at ~60 ps delay persists independent of the pump fluence.

A micromagnetic model was constructed in which the superlattice was treated as a one-dimensional chain of macrospins with the thickness of each equal to one half of the lattice constant of the large Laves phase unit cell. A bilayer of one hard (h) and one soft (s) layer was constructed with the top and bottom surfaces of the bilayer joined together to represent a superlattice of infinite extent. The model solves a set of Landau-Lifshitz-Gilbert equations (see Supplemental Material [21]), for the magnetization $\mathbf{M}$ of each macrospin, that are coupled by the exchange torques acting between adjacent macrospins, $\mathbf{N}_{\text{exch}}$,

$$\frac{\partial \mathbf{M}}{\partial t} = -|\gamma|(\mathbf{M} \times \mathbf{H}_{\text{eff}} + \mathbf{N}_{\text{exch}}) + \frac{\alpha}{M}\mathbf{M} \times \frac{\partial \mathbf{M}}{\partial t}. \quad (2)$$

The effective field, $\mathbf{H}_{\text{eff}}$, contains contributions from the Zeeman interaction and magnetocrystalline anisotropy (K), while α and γ are the Gilbert damping parameter and gyromagnetic ratio, respectively. Values for the magnetization ($M_s = 490$, $M_h = 760$ emu/cm^3), uniaxial magnetocrystalline anisotropy constant ($K_s = 1 \times 10^2$, $K_h = 7 \times 10^5$ J/m^3) and intralayer ($A_{s,h} = 1.5 \times 10^{-11}$ J/m) and interlayer ($A_I = -1.5 \times 10^{-11}$ J/m) exchange constants were taken from a previous micromagnetic calculation [22]. The layer thicknesses ($d_h = 22.5$ Å, $d_s = 82.5$ Å) are integer multiples of the lattice constant (7.5 Å) and lie close to the experimental values. The moments were initially set in the giant ferrimagnetic state with the net moment along the positive x, easy axis,

direction (see Fig. 1, inset). The bias field was applied 1° from the easy axis to obtain a unique equilibrium state.

A simulated magnetization curve is shown in Fig. 1(a). The soft-layer exchange constant was reduced significantly to 2×10^{-12} J/m to obtain a bending field close to the experimental value. This reduced exchange constant is an effective micromagnetic value that accounts for the effect of finite temperature [23,24]. No switching of the hard layer is observed, even when the field is increased by a further order of magnitude to that shown, unless the soft layer exchange constant is increased significantly. Switching of the hard layer is mediated by both the presence of defects and finite temperature, neither of which are included in the model.

The effect of optical pumping was simulated as an instantaneous reduction of the magnetization values ($\Delta M_{s,h}$), hard-layer anisotropy constant (ΔK_h), and exchange constants ($\Delta A_{s,h,I}$). The anisotropy of the soft YFe_2 layers was assumed to be negligible. Each parameter was allowed to relax exponentially to its equilibrium value with a time constant of 250 ps. Initially the damping parameter was set to a low value of 0.05 to assist in the identification of the resonance modes. The frequency of the dominant mode within the soft layer was found to lie close to that of the measured oscillations, while the dominant mode within the hard layer had an order of magnitude higher frequency. The soft-layer damping constant was then increased to 0.1 and the hard-layer value to 0.3, the latter to reflect the expected large damping of the $DyFe_2$ layers and to suppress the appearance of hard-layer precession in the simulated response in agreement with experiment.

Figure 4 shows the time evolution of the average value of M_x for the hard and soft layers as the bias field H is increased. The value of $\Delta M_{s,h} = 20\%$ is close to that measured for a pump fluence of 2.0 mJ/cm^2, while the values of $\Delta K_h = 90\%$ and $\Delta A_{s,h,I} = 10\%$ were found to best reproduce the three principal features of the TRMOKE data discussed previously. It is well known [25] that the temperature dependence of the magnetic anisotropy varies as a high power of the magnetization, and strong temperature dependence of the $DyFe_2$ magnetic anisotropy has been observed previously in $DyFe_2$-YFe_2 superlattices. The field dependence of the oscillation frequency is in good agreement with experiment [see Fig. 2(c)]. The nonoscillatory background gradually changes sign with increasing field as the contribution of the changing bending angle dominates that of the demagnetization. An inflection, highlighted by a vertical dashed line in Fig. 4(a), is observed at similar time delay to that at which an inflection is observed within the TRMOKE data. The appearance of this feature in the soft-layer response corresponds to a peak in the hard layer, shown in Fig. 4(b), which arises when a sufficiently large reduction of K_h allows the torque generated by the spring to reorient the hard-layer

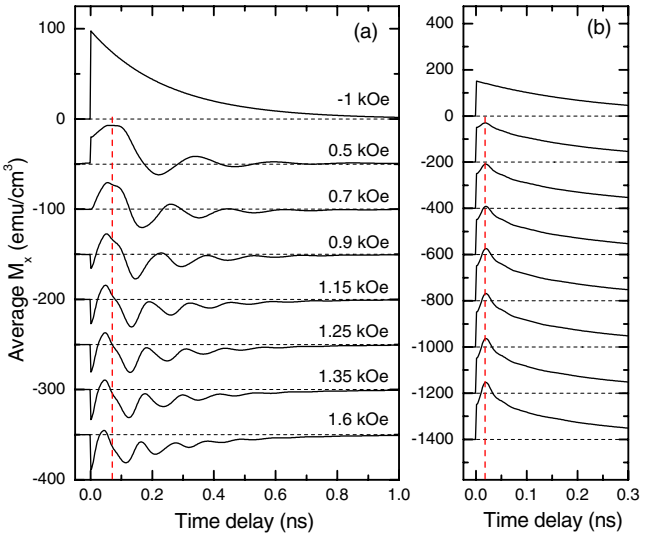

FIG. 4 (color online). Micromagnetic simulations of the average value of M_x within (a) the soft layer and (b) the hard layer for pump-induced changes of $\Delta M = 20\%$, $\Delta K_h = 90\%$ and $\Delta A = 10\%$ within both layers. The vertical dashed lines highlight the reorientation of the hard layer.

magnetization. The maximum hard-layer deflection occurs at a delay of ~17 ps, earlier than the inflection at ~60 ps in the soft-layer response. This delay corresponds to the time taken for the deflection of the moments at the interface to propagate to the center of the soft layer. (The propagation of the reorientation through the bilayer can be clearly seen in animations of the simulation data, included in the Supplemental Material [21].) The value of ΔA was found to affect the oscillation amplitude of the soft layer, a value of 10% yielding reasonable agreement with experiment. Animations of the simulation data are included in the Supplemental Material [21] that illustrate clearly the mechanism driving the dynamics and the hard-layer moment reorientation.

Further simulations with $\Delta K_h \geq 97\%$ showed that switching to the giant ferrimagnetic state may occur but is sensitive to the precession frequency which depends upon the value of the applied field (see Supplemental Material [21]). Crossing of the hard axis due to precession must be synchronized with substantial recovery of the hard-layer anisotropy if switching is to occur. The switching process is also sensitive to the temperature dependence of the damping, which was not included in the simulations. No evidence of switching was observed in the experiment, and further studies are required to identify the optimum conditions for switching.

In summary, TRMOKE measurements have revealed the optically induced parametric excitation of magnetization dynamics within a $[DyFe_2(20\,\text{Å})/YFe_2(80\,\text{Å})]_{\times 40}$ exchange spring superlattice. The experimental results are reproduced by micromagnetic simulations that reveal winding and precession within the soft-layer spring structure, and

reorientation of the hard-layer magnetization. For sufficiently large pump fluence switching of the hard-layer magnetization may be induced, which has applications in data storage technology and suggests opportunities for optically induced switching in other physical systems.

*L.R.Shelford@exeter.ac.uk

[1] G. J. Bowden, J.-M. L. Beaujour, S. Gordeev, P. A. J. de Groot, B. D. Rainford, and M. Sawicki, J. Phys. Condens. Matter **12**, 9335 (2000).

[2] D. Suess, T. Schrefl, S. Fähler, M. Kirschner, G. Hrkac, F. Dorfbauer, and J. Fidler, Appl. Phys. Lett. **87**, 012504 (2005).

[3] D. Suess, J. Magn. Magn. Mater. **308**, 183 (2007).

[4] J. U. Thiele, S. Maat, J. L. Robertson, and E. E. Fullerton, IEEE Trans. Magn. **40**, 2537 (2004).

[5] M. Sawicki, G. J. Bowden, P. A. J. de Groot, B. D. Rainford, and J.-M. L. Beaujour, Appl. Phys. Lett. **77**, 573 (2000).

[6] J.-M. L. Beaujour, S. N. Gordeev, G. J. Bowden, P. A. J. de Groot, B. D. Rainford, R. C. C. Ward, and M. R. Wells, Appl. Phys. Lett. **78**, 964 (2001).

[7] S. N. Gordeev, J.-M. L. Beaujour, G. J. Bowden, B. D. Rainford, P. A. J. de Groot, R. C. C. Ward, M. R. Wells, and A. G. M. Jansen, Phys. Rev. Lett. **87**, 186808 (2001).

[8] M. Grimsditch, R. Camley, E. E. Fullerton, S. Jiang, S. D. Bader, and C. H. Sowers, J. Appl. Phys. **85**, 5901 (1999).

[9] D. S. Schmool, Nanosci. Nanotechnol. Lett. **3**, 515 (2011).

[10] M. Franchin, J. P. Zimmermann, T. Fischbacher, G. Bordignon, P. A. J. de Groot, and H. Fangohr, IEEE Trans. Magn. **43**, 2887 (2007).

[11] M. A. Bashir, T. Schrefl, J. Dead, A. Goncharov, G. Hrkac, S. Bance, D. Allwood, and D. Suess, IEEE Trans. Magn. **44**, 3519 (2008).

[12] T. J. Fal, K. L. Livesey, and R. E. Camley, J. Appl. Phys. **109**, 093911 (2011).

[13] M. J. Bentall, R. C. C. Ward, E. J. Grier, and M. R. Wells, J. Phys. Condens. Matter **15**, 6493 (2003).

[14] K. N. Martin, P. A. J. de Groot, B. D. Rainford, K. Wang, G. J. Bowden, J. P. Zimmermann, and H. Fangohr, J. Phys. Condens. Matter **18**, 459 (2006).

[15] G. J. Bowden, P. A. J. de Groot, B. D. Rainford, K. Wang, K. N. Martin, J. P. Zimmermann, and H. Fangohr, J. Phys. Condens. Matter **18**, 5861 (2006).

[16] K. Dumesnil, M. Dutheil, C. Dufour, and P. Mangin, Phys. Rev. B **62**, 1136 (2000).

[17] G. J. Bowden, J.-M. L. Beaujour, A. A. Zhukov, B. D. Rainford, P. A. J. de Groot, R. C. C. Ward, and M. R. Wells, J. Appl. Phys. **93**, 6480 (2003).

[18] K. Dumesnil, C. Dufour, P. Mangin, A. Rogalev, and F. Wilhelm, J. Phys. Condens. Matter **17**, L215 (2005).

[19] A. Kirilyuk, A. Kimel, and T. Rasing, Rev. Mod. Phys. **82**, 2731 (2010).

[20] Y. Liu, L. R. Shelford, V. V. Kruglyak, R. J. Hicken, Y. Sakuraba, M. Oogane, and Y. Ando, Phys. Rev. B **81**, 094402 (2010).

[21] See Supplemental Material at http://link.aps.org/supplemental/10.1103/PhysRevLett.113.067601 for details of measurements of ultrafast laser demagnetization and for more details of the micromagnetic simulations including animations of the simulated dynamics and an example of switching.

[22] D. Wang, C. G. Morrison, A. R. Buckingham, G. J. Bowden, R. C. C. Ward, and P. A. J. de Groot, J. Magn. Magn. Mater. **321**, 586 (2009).

[23] G. Vértesy and I. Tomáš, J. Appl. Phys. **93**, 4040 (2003).

[24] U. Atxitia, D. Hinzke, O. Chubykalo-Fesenko, U. Nowak, H. Kachkachi, O. N. Mryasov, R. F. Evans, and R. W. Chantrell, Phys. Rev. B **82**, 134440 (2010).

[25] A. H. Morrish, *The Physical Principles of Magnetism* (Wiley, New York, 1965).